Macromolecules

ARTICLE

pubs.acs.org/Macromolecules

Super Gas Barrier of All-Polymer Multilayer Thin Films

You-Hao Yang, Merid Haile, Yong Tae Park, Frank A. Malek, and Jaime C. Grunlan*

Department of Chemical Engineering, Texas A&M University, College Station, Texas 77843, United States

ABSTRACT: Thin film assemblies of branched polyethylenimine (PEI) and poly(acrylic acid) (PAA), deposited using the layer-by-layer technique, were studied in an effort to produce all-polymer thin films with low oxygen permeability. Altering the pH of PEI and PAA results in large thickness variations (from 90 nm to 4.74 μm for 30-bilayer films). Cross-linking these films with glutaraldehyde (GA) create an inhibition of polymer interdiffusion, causing exponential film growth to be reset. AFM images show the surface morphology of PEI/PAA assemblies can be controlled by the pH and the final polymer layer deposited, with surface roughness ranging from 2.1 to 49.1 nm. Most pH combinations failed to produce a film with high oxygen barrier, but 8 bilayers of PEI at pH 10 and PAA at pH 4 produce a 305 nm thick film with an oxygen transmission rate below 0.005 cm^3/(m^2 day). This unique thin film barrier (P_{O_2} < 3.2 × 10^{-21} cm^3 (STP) cm/(cm^2 s Pa)) is a promising alternative to current polymeric membranes, flexible electronics, and food packaging materials.

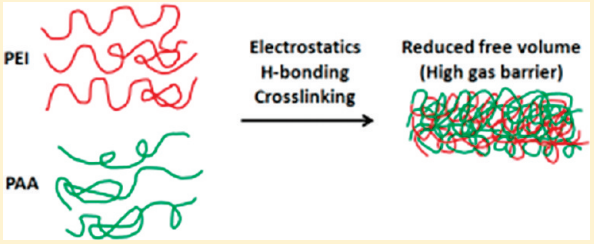

INTRODUCTION

As the modern layer-by-layer (LbL) assembly technique approaches its 20-year anniversary,[1,2] it has grown to become one of the most studied thin film fabrication methods because of its simplicity, robustness, and tailorability.[3−5] LbL can be used to deposit a variety of ingredients that include polymers,[6−8] quantum dots,[9,10] nanoparticles (including spheres, rods, tubes, and plates),[11−20] organic dyes,[21] dendrimers,[22] and biological molecules (including peptides, DNA, proteins, and viruses).[23−31] The functionality, morphology, and structure of LbL films can be easily tailored by changing molecular weight,[32,33] concentration,[34] chemistry,[35] pH,[34,36] ionic strength,[34,37] temperature,[38,39] and deposition time[34,40,41] of deposited species and their aqueous solutions or suspensions (in the case of particles). Using different components with specific interactions, such as electrostatic attraction or hydrogen bonding, the complementary ingredients attract each other and form a multilayered structure. In two-component systems, each deposition of both ingredients is referred to as a bilayer (BL). The versatility of LbL assembly makes it a good candidate for surface applications that include gas barrier coatings,[42] superhydrophobicity,[43−45] antimicrobials,[46−48] drug delivery,[49−51] electrical conductivity,[12,52,53] selective area patterning,[11,54,55] and battery electrolytes.[56]

Many LbL systems show linear growth as a function of layers deposited, but those containing weak polyelectrolytes (e.g., polyethylenimine (PEI) and poly(acrylic acid) (PAA)) often exhibit exponential growth.[40,57] It is suggested that this exponential thickening effect comes from an "in and out" diffusion mechanism,[25,58,59] involving an endothermic polycation/polyanion complexation process.[60] Polymer chains not only adsorb onto the film's surface but also interpenetrate into inner layers for charge overcompensation, which exponentially increases the total film thickness. Weak polyelectrolyte multilayer assemblies have been widely studied because the charge density along the polymer chain can be altered with pH.[36,42,61] Previous research using poly(allylamine hydrochloride) (PAH) and PAA shows the ability to systematically control the thickness, density, composition, and wettability by simply changing the charge density of these polyelectrolytes.[8,36,62] The ability to tailor charge density with pH provides a more tailorable LbL process. More recently, this concept was applied to clay−polymer assemblies that exhibit tunable gas permeability by changing the charge density of PEI.[42] The resulting nanobrick wall structure exhibits high oxygen barrier that is unrivaled by any other type of polymer or composite (or even SiO_x).

In an effort to find an all-polymer multilayer gas barrier, PEI/PAA assemblies with different pH combinations (10/4, 8/6, 7/7, and 4/4) were studied. Thickness, density, microstructure, and oxygen permeability can all be tailored by changing the pH values of aqueous PEI and PAA solutions. The thickest films are produced when both polymers have the lowest charge (10/4 for PEI/PAA), whereas the highly charged combination (7/7) is the thinnest. Cross-sectional TEM shows a homogeneous structure without any discernible boundaries between layers in any of the films. The thickest PEI/PAA film (~1 μm thick at 10BL) exhibits an undetectable oxygen transmission rate (<0.005 cm^3/(m^2 day)), while maintaining complete transparency. These films were cross-linked using glutaraldehyde (GA) to reduce moisture sensitivity. The cross-linked 8BL PEI/PAA (10/4) coating exhibits a permeability under 3.2 × 10^{-21} cm^3 (STP) cm/(cm^2 s Pa), which is believed to be the lowest permeability of an all-polymer LbL system ever reported. Although oxygen permeability of this system is higher than polymer−clay assemblies (due to layer thickness),[42] it requires fewer layers to achieve

Received: November 16, 2010
Revised: January 21, 2011
Published: February 21, 2011

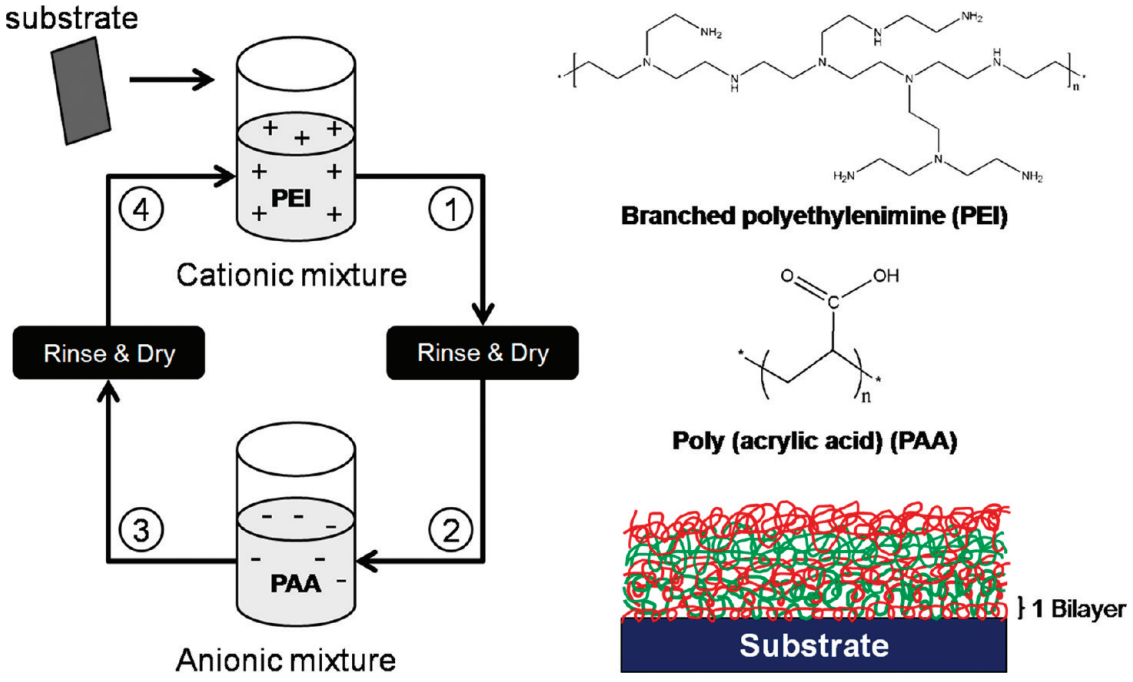

Figure 1. Schematic of the layer-by-layer deposition process. Steps 1−4 are repeated until the desired number of PEI/PAA bilayers is deposited.

a high oxygen barrier. This relatively simple recipe may be of use for a variety of packaging applications, including flexible electronics that require high flexibility and transparency (in addition to high barrier).

EXPERIMENTAL DETAILS

Materials. Branched polyethylenimine (PEI) (Aldrich, St. Louis, MO) ($M_W \sim 25\,000$ g/mol) was chosen as the cationic polymer and dissolved into 18.2 MΩ deionized water to create a 0.1 wt % solution. The pH was adjusted from its unaltered value (~10.5) to 10, 8, 7, and 4 by adding 1.0 M hydrochloric acid (HCl). Poly(acrylic acid) (PAA) (Aldrich) ($M_W \sim 100\,000$ g/mol) was the anionic polymer that was used as a 0.2 wt % solution with 18.2 MΩ deionized water. The pH of PAA was adjusted from its unaltered value (~3.1) by adding 1.0 M sodium hydroxide (NaOH). Glutaraldyhyde (GA) (Aldrich) was used as a cross-linker for PEI/PAA assemblies, in the form of 1.0 wt % aqueous solution.

Substrates. Single-side-polished (100) silicon wafers (University Wafer, South Boston, MA) were used as deposition substrates for ellipsometry, profilometry, and atomic force microscopy (AFM). Silicon wafers were piranha treated with 3:1 30% hydrogen peroxide to 99% sulfuric acid ratio and stored in deionized water before being used. *Caution: piranha solution reacts violently with organic material and needs to be handled properly*. Prior to use, the silicon wafers were rinsed with acetone and deionized water. Poly(ethylene terephthalate) (PET) film with a thickness of 179 μm (trade name ST505, Dupont−Teijin) was purchased from Tekra (New Berlin, WI). A 175 μm polystyrene (PS) film (Goodfellow, Oakdale, PA) was used as a substrate for transmission electron microscopy (TEM). Both PET and PS films were rinsed with deionized water and methanol before use. Cleaned PET and PS substrates were then corona-treated with a BD-20C corona treater (Electro-Technic Products Inc., Chicago, IL). Corona treatment improves adhesion of the first polyelectrolyte layer by oxidizing the film surface.[63] Polished Ti/Au crystals with a resonance frequency of 5 MHz were purchased from Maxtek, Inc. (Cypress, CA), and used as deposition substrates for quartz crystal microbalance (QCM) characterization.

Layer-by-Layer Deposition. The overall layer-by-layer process is shown schematically in Figure 1. A given substrate was first dipped into the PEI solution for 5 min, followed by rinsing with deionized water for 30 s and drying with a stream of filtered air. After the first positively charged layer was adsorbed, the substrate was dipped into PAA solution for another 5 min, followed by another rinsing and drying cycle. Starting from the second deposition cycle, the remaining numbers of bilayers were created using 1 min dip times. This process was carried out using home-built robot systems.[64,65] The pH of PEI or PAA is abbreviated next to their name in the figures and text. For example, one bilayer of PEI(pH = 10)/PAA(pH = 4) is abbreviated as $(PEI_{10}/PAA_4)_1$.

Film Characterization. Assembly thickness on silicon wafers was measured every five bilayers with a PHE-101 discrete wavelength ellipsometer (Microphotonics, Allentown, PA). A 632.8 nm laser was used at an incidence angle of 65°. For the PEI_{10}/PAA_4 system, thickness was measured with a P-6 profilometer (KLA-Tencor, Milpitas, CA). The average thickness was calculated from three 0.01 m 2-D measurements. Mass increments were measured each layer with a research quartz crystal microbalance (QCM) (Inficon, East Sycrase, NY) with a frequency range of 3.8−6 MHz. The 5 MHz quartz crystal was inserted in a holder and dipped into the PEI and PAA solutions. After each deposition, the crystal was rinsed and dried and then left on the microbalance to stabilize for 5 min. Fourier transform infrared spectra were obtained by an ALPHA FTIR spectrometer (Bruker Optics Inc., Billerica, MA) with a universal sampling module. Cross sections of the PEI/PAA assemblies were imaged with a JEOL 1200 EX TEM (Mitaka, Tokyo, Japan), operated at 110 kV. Samples were prepared for imaging by embedding a piece of PS, supporting the LbL film, in epoxy prior to sectioning it with a diamond knife. Surface structure of the coated silicon wafers were imaged with a multimode scanning probe microscope (SPM) (Veeco Digital Instruments, Santa Barbara, CA) in tapping mode. OTR testing was performed by MOCON (Minneapolis, MN) in accordance with ASTM D-3985,[66] using an Oxtran 2/21 ML instrument at 23 °C and 0% or 100% RH. Glass transition temperature (T_g) was measured by a Q20 differential scanning calorimeter (DSC) (TA Instruments, New Castle,

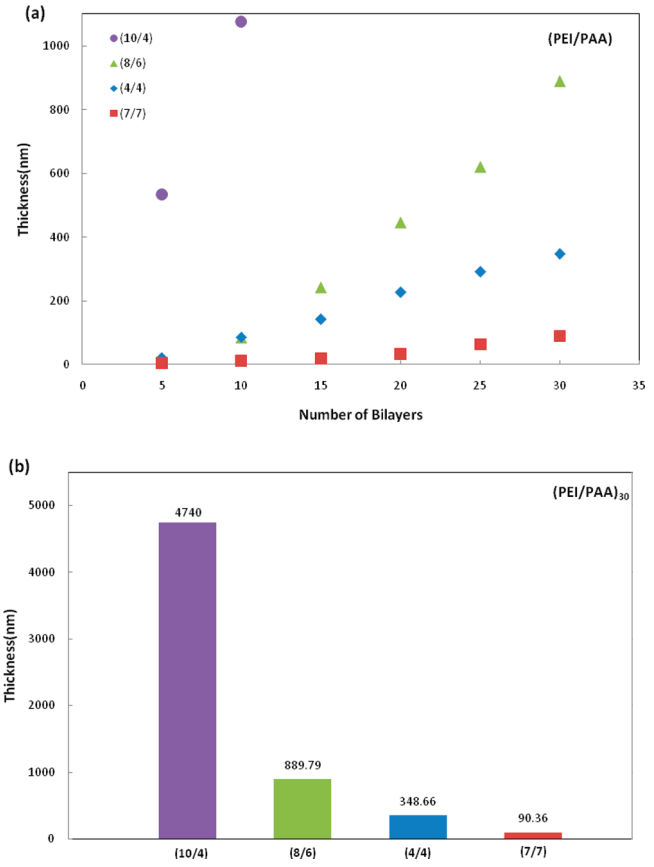

Figure 2. Film thickness as a function of bilayers deposited for LbL assemblies made with varying pH combinations of PEI and PAA (a). Thickness of 30BL PEI/PAA films with varying pH combinations (b). The numbers in parentheses are the deposition pH of PEI and PAA solutions, respectively.

DE). 5−10 mg samples were placed in aluminum pans and scanned from −50 to 150 °C at a heating and cooling rate of 10 °C/min.

RESULTS AND DISCUSSION

Film Growth. Film growth of four different PEI/PAA pH combinations (PEI_4/PAA_4, PEI_7/PAA_7, PEI_8/PAA_6, and PEI_{10}/PAA_4) was measured by ellipsometry and profilometry, as shown in Figure 2. The growth rate of PEI_{10}/PAA_4 is the greatest (thickest) among all the pH combinations studied, achieving a thickness of 4.74 μm at 30 bilayers. The thickness order of the rest of pH combinations is 8/6 (890 nm) > 4/4 (349 nm) > 7/7 (90 nm) (Figure 2b). These thickness differences primarily attributed to two factors: (1) the inherent pH-responsive morphology of the weak polyelectrolytes and (2) the interactive charge overcompensation from the basic PEI and acidic PAA solutions. As these polymers become highly charged (at low pH for PEI and high for PAA), they undergo intrasegmental repulsion and deposit thinner layers. With lower charge, PEI and PAA remain more loopy or coiled due to intramolecular van der Waal attractions.[36] In terms of interactive charge overcompensation, the pK_a of PAA is very sensitive to local pH,[36,62] so the basic PEI solution will make PAA segments more charged. The same scenario occurs with PEI, which exhibits an increased charge density when exposed to the acidic PAA solution. Once the charge density is increased, more charged groups are needed for

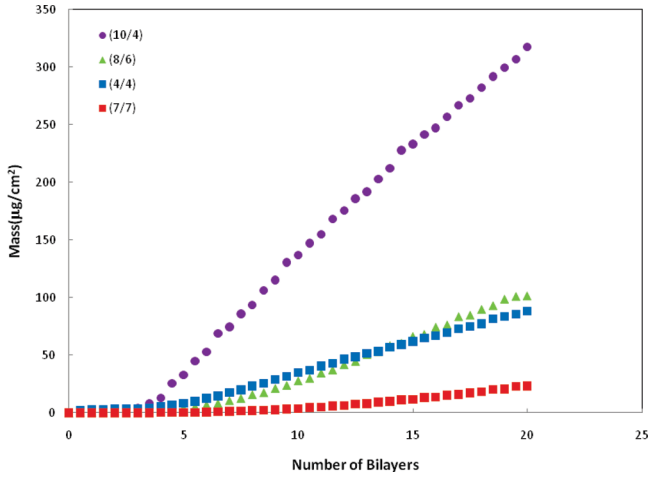

Figure 3. Mass as a function of layers deposited for assemblies made with varying pH combinations of PEI and PAA.

overcompensation. As this process continues, with each deposition step, more PEI and PAA are adsorbed, resulting in the dramatic increase in film thickness as a function of layers deposited.

It is interesting to observe that $(PEI_8/PAA_6)_{30}$ is 155% thicker than $(PEI_4/PAA_4)_{30}$ (Figure 2b). Considering the inherent pH-responsive morphology of these polymers, PEI(pH = 8) has a more loopy/coiled conformation than PEI(pH = 4) and PAA-(pH = 4) has a more loopy/coiled conformation than PAA(pH = 6). In (8/6), the nonioinized segments of PEI or PAA are continuously titrated by the oppositely charged polymer solution during the deposition process. This titration process results in more charged groups from PEI and PAA being required for charge overcompensation, which adds more PEI and PAA chains and results in a thicker film. For (4/4), the local titration is expected to have less impact than (8/6). In other words, the overall (4/4) film thickness is primarily controlled by the intrinsic conformations of PEI and PAA. For (7/7), both PEI and PAA are in their highly charged state, without the influence of local titration, which results in the smallest thickness (90 nm) for 30 bilayers. The fact that the thickness of $(PEI/PAA)_{30}$ can be altered by nearly 2 orders of magnitude, from 4.74 μm to 90 nm by simply changing the pH, highlights the significant tailorability of these LbL assembled thin films.

The mass of each deposited polymer layer was measured with a QCM, as shown in Figure 3. Similar to the observed thickness growth (Figure 2a), the mass increase as a function of layers deposited is greatest for the PEI_{10}/PAA_4 system. In the case of mass, the growth is initially not linear but gradually becomes more linear (as observed by others).[28] The PEI_8/PAA_6 and PEI_4/PAA_4 systems exhibit similar growth, while PEI_7/PAA_7 again shows the least growth relative to all other pH combinations. The average mass deposited for each PEI_{10}/PAA_4 bilayer is 15.9 $\mu g/cm^2$, which is about 3 times higher than PEI_8/PAA_6 (~5.1 $\mu g/cm^2$) and PEI_4/PAA_4 (~4.4 $\mu g/cm^2$). As for PEI_7/PAA_7, there is only 1.2 $\mu g/cm^2$ deposited every bilayer. The dramatic difference between 10/4 and 8/6 come from the interactive charge overcompensation described above. A smaller pH difference for 8/6, relative to 10/4, causes the amount of charged groups ionized by the oppositely charged polymer solution to also be smaller. This reduced level of ionization requires fewer polymer chains to be needed for charge

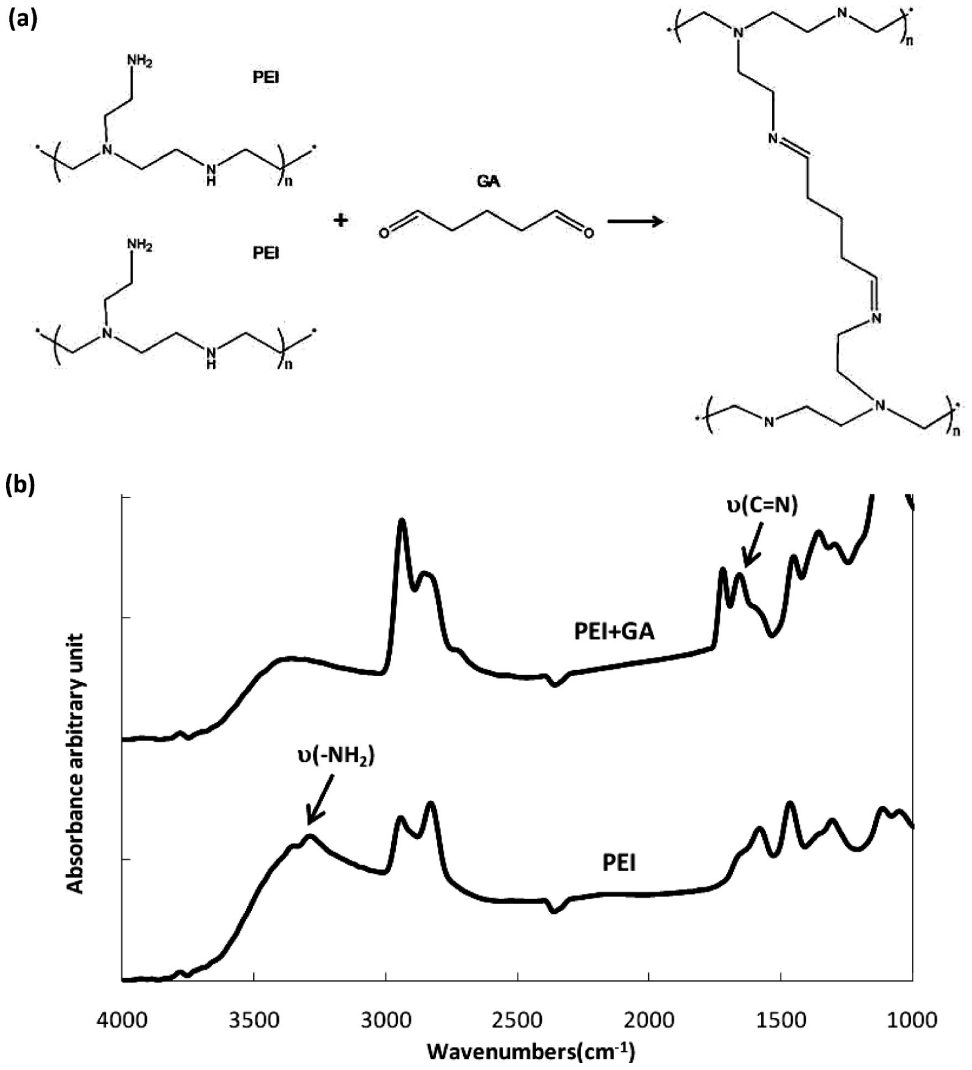

Figure 4. Cross-linking mechanism of PEI and GA (a). FTIR spectra of PEI and PEI cross-linked with GA (b). These spectra are intentionally overlaid with arbitrary offset for clarity.

overcompensation, in the 8/6 system, resulting in reduced mass growth relative to 10/4. In addition to verifying growth, QCM provides the composition of each pH combination. PEI_{10}/PAA_4 is 58 wt % PEI (average value for measurements between 10 and 20 BL), while PEI_8/PAA_6 contains only 31 wt % PEI. PEI_4/PAA_4 and PEI_7/PAA_7 have 46 and 71 wt % PEI, respectively. The dramatic composition change from 8/6 to 7/7 shows that although the charge densities of PEI and PAA both increase from 8/6 to 7/7, the adsorption of charged PAA is weaker than charged PEI.

Influence of Cross-Linking on Film Growth. Glutaraldehyde (GA) was used to cross-link these PEI/PAA assemblies every 10 bilayers. The presumed mechanism of cross-linking is shown in Figure 4a. Uncharged primary amine groups from PEI are cross-linked by forming N═C bonds (Schiff base) with glutaraldehyde.[67] FTIR spectroscopy was used to confirm this reaction by showing a smaller peak for cross-linked PEI near 3300 cm^{-1} ($-NH_2$ stretching band), as shown in Figure 4b. Around 1670 cm^{-1}, a new peak is created by the PEI + GA reaction (N═C stretching band), which indicates the generation of a Schiff base.

Figure 5 compares thickness growth with and without GA cross-linking. In all four systems, the films grow exponentially (or superlinearly) with and without cross-linking and all cross-linked systems are thinner than their un-cross-linked counterparts. These thickness trends suggest that different pH combinations exhibit different extents of cross-linking. The 30BL PEI_4/PAA_4 film exhibits an 11% thickness reduction, following cross-linking every 10 bilayers, relative to an un-cross-linked film. For the same number of bilayers, PEI_7/PAA_7, PEI_8/PAA_6, and PEI_{10}/PAA_4 shrink by 22.2, 42.4, and 58.2%, respectively. The higher the pH of PEI, the greater the loss in thickness due to glutaraldehyde's ability to cross-link the free primary amine groups. As the pH of PEI increases, so does the number of reactive, uncharged primary amine groups of PEI that leads to a tighter network and thinner resulting films. Figure 5e shows the mass increase for every bilayer of $(PEI_{10}/PAA_4)_{30}$, with cross-linking at 10 and 20 BL. The two plateaus at 10 and 20 BL clearly demonstrate the inhibition effect of cross-linking that effectively "resets" the film growth. A similar inhibition effect, caused by creating a "blocking layer", has been observed by others.[68,69] Cross-linking prevents interdiffusion of polymers into the underlying layers, which causes the growth to start over again (as though deposition were occurring on a bare substrate). This ability to reset the exponential growth process at a desired number of bilayers is another tool for tailoring LbL film thickness and properties.

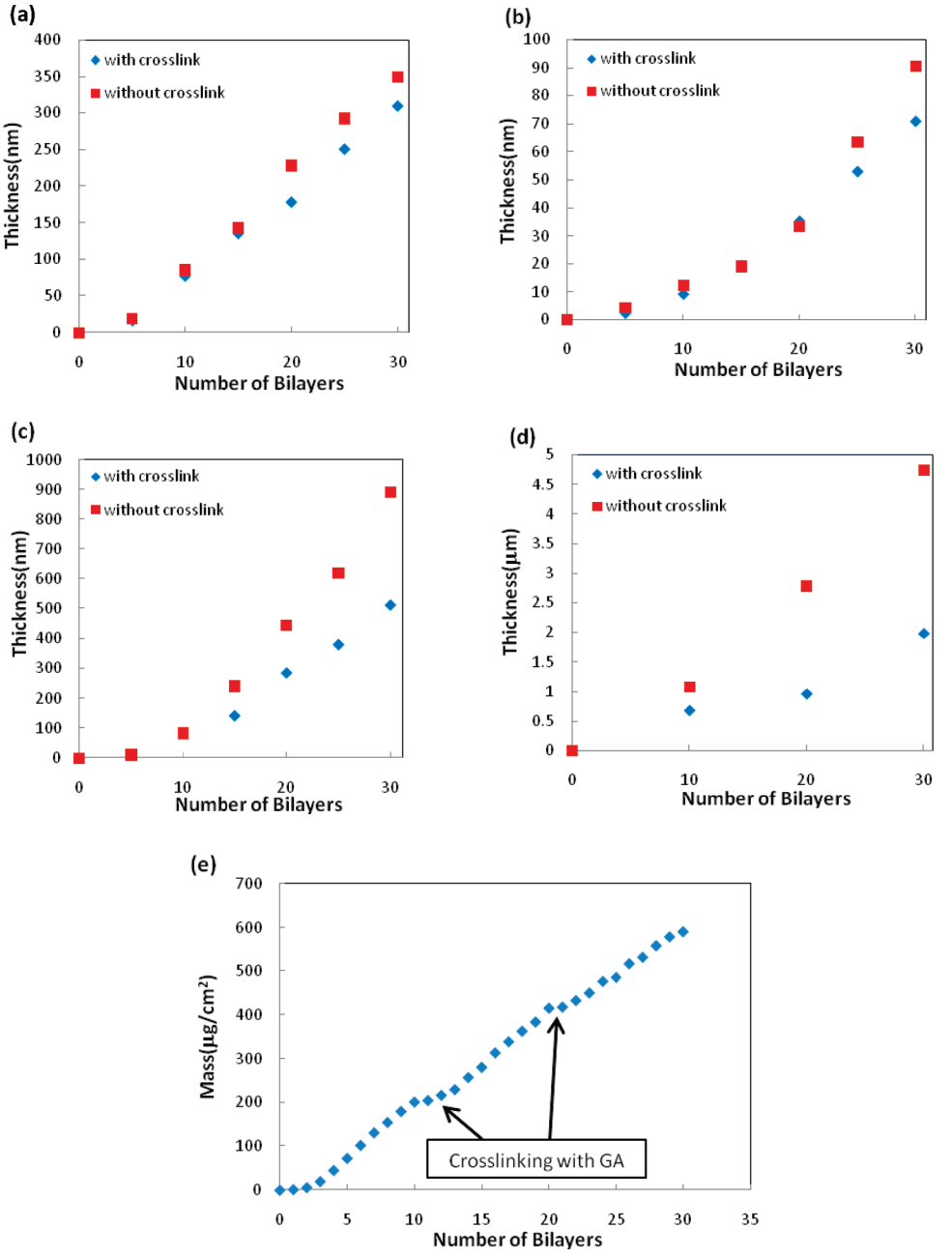

Figure 5. Film thickness as a function of bilayers deposited for LbL assemblies made with PEI_4/PAA_4 (a), PEI_7/PAA_7 (b), PEI_8/PAA_6, (c), and PEI_{10}/PAA_4 (d). (a−c) were measured with ellipsometry, while (d) was measured with profilometry. Mass as a function of deposited bilayers, for a 30 BL PEI_{10}/PAA_4 film (e), is shown to highlight the reset of film growth at 10 and 20 BL.

Film Morphology. TEM cross-sectional images of $(PEI/PAA)_{20}$, made with various pH combinations, are shown in Figure 6. All four films were deposited on PS to facilitate sectioning. These images show the difference in thickness, with regard to pH combinations, that was discussed in the previous sections. The thickness order is PEI_{10}/PAA_4 > PEI_8/PAA_6 > PEI_4/PAA_4 > PEI_7/PAA_7, which agrees with ellipsometer and profilometer measurements (Figure 2). The homogeneity of these images suggests a high level of interdiffusion between PEI and PAA that eliminates the boundaries between each layer.

AFM surface images of $(PEI/PAA)_{10}$ and $(PEI/PAA)_{10.5}$ are shown in Figure 7. $(PEI_8/PAA_6)_{10}$ (Figure 7b) and $(PEI_7/PAA_7)_{10}$ (Figure 7c) both exhibit smooth surfaces, while $(PEI_{10}/PAA_4)_{10}$ (Figure 7a) and $(PEI_4/PAA_4)_{10}$ (Figure 7d) have an ordered surface texture. Both polymers in PEI_{10}/PAA_4 have low charge, which results in a more interdiffused morphology. During layer-by-layer assembly, these two globular polymers enhance the uneven topography that occurs in all films. PEI_8/PAA_6 and PEI_7/PAA_7, with more highly charged polymers, exhibit a smoother surface due to more extended (thinner) polymer chains. As for PEI_4/PAA_4, with a combination of highly charged PEI and weakly charged PAA, there is a reduced texture relative to PEI_{10}/PAA_4. With PAA in the outmost layer, this texture is enhanced. On the other hand, PEI in its highly charged state effectively suppresses the texture, as evidenced by the

dx.doi.org/10.1021/ma1026127 |*Macromolecules* 2011, 44, 1450–1459

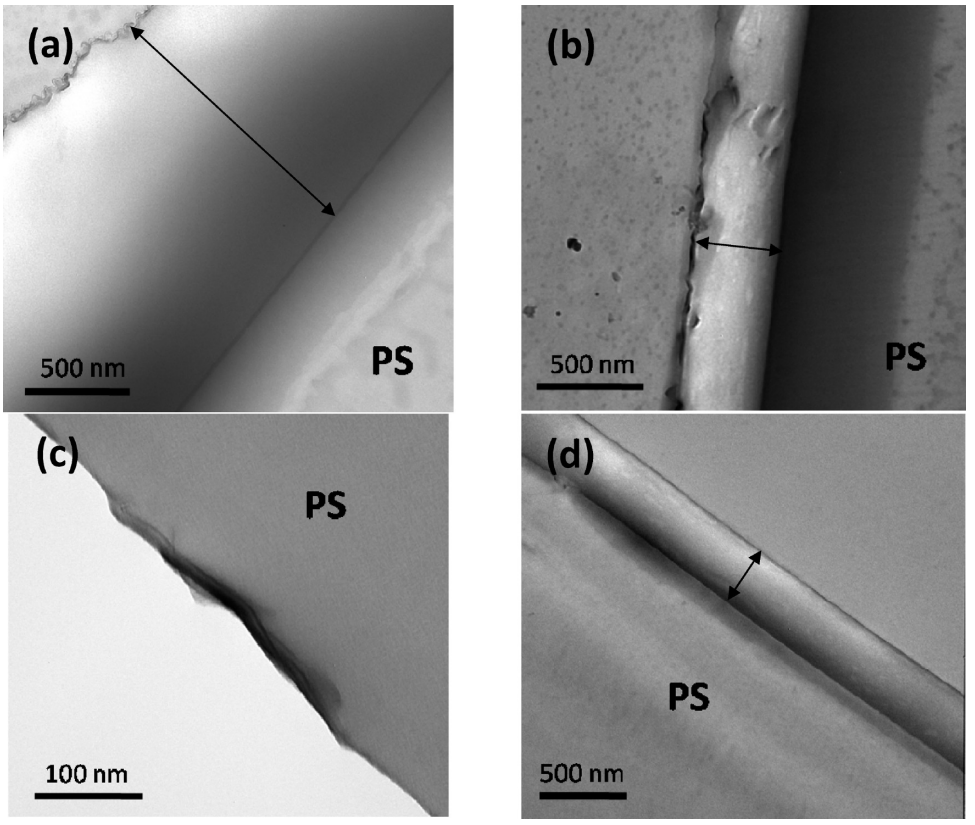

Figure 6. TEM cross-sectional images of $(PEI/PAA)_{20}$ on PS made with various pH combinations: PEI_{10}/PAA_4 (a), PEI_8/PAA_6 (b), PEI_7/PAA_7 (c), and PEI_4/PAA_4 (d). The double arrow bars highlight the thickness of the films.

relatively smooth surface of $(PEI_4/PAA_4)_{10.5}$ (Figure 7f), in which the outmost layer is PEI instead of PAA. Even for relatively rough $(PEI_{10}/PAA_4)_{10.5}$ (Figure 7e), the outer PEI layer seems to cover up most of the surface texture.

In general, higher charged polymer combinations have smoother surfaces and less charged combinations have rougher surfaces. The order of surface roughness is PEI_{10}/PAA_4 (49.1 nm) > PEI_4/PAA_4 (5.9 nm) > PEI_8/PAA_6 (4.3 nm) > PEI_7/PAA_7 (2.1 nm), which were all calculated using a 20 μm × 20 μm area. For 10.5 bilayers, the change of surface organization due to the outmost layer can be clearly seen. In PEI_{10}/PAA_4, the less charged PEI covers up the rough surface created by weakly charged PAA that decreases the surface roughness 42% (from 49.1 to 28.3 nm). On the other hand, when the outmost layer of PEI_4/PAA_4 is changed from a less charged PAA to highly charged PEI, there is a 25% decrease in surface roughness (from 5.9 to 4.4 nm). From the above results, two things can be inferred: (1) in a weakly charged state, PEI creates a smoother surface than PAA and (2) interdiffusion of PEI and PAA will not change the surface morphology dictated by the outmost layer. One can control the surface roughness of PEI/PAA assemblies simply by changing the charge density of each polymer and the outmost layer, which could be useful for self-healing and superhydrophobic films. In the present study, it is low oxygen permeability that is being sought.

Oxygen Barrier. Oxygen transmission rates for PEI_8/PAA_6, PEI_7/PAA_7, and PEI_4/PAA_4 films show little improvement relative to uncoated PET (OTR > 8.45 $cm^3/(m^2$ day) for assemblies on 175 μm thick PET film). Only the PEI_{10}/PAA_4 system exhibits low OTR with fewer than 10 bilayers, as summarized in Table 1 and Figure 8. Various numbers of bilayers and cross-linking conditions were tested at 23 °C and 0 or 100% RH. In the case of 0% RH, 8BL films (cross-linked and un-cross-linked) achieve an undetectable oxygen transmission rate (<0.005 $cm^3/(m^2$ day)), which is more than 3 orders of magnitude lower than uncoated PET film (OTR = 8.48 $cm^3/(m^2$ day)). Even a cross-linked 6BL film exhibits an OTR that is an order of magnitude better than the substrate (0.56 $cm^3/(m^2$ day)) (Figure 8a). In the case of 100% RH, the OTR of an 8BL film increases from undetectable (<0.005) to 0.09 $cm^3/(m^2$ day), while the other systems exhibit significantly higher values than at 0% RH (Figure 8b). At 10 bilayers, the un-cross-linked film maintains an undetectable OTR at 100% RH (Table 1), while the OTR of the cross-linked film increases from undetectable (<0.005) to 0.07 $cm^3/(m^2$ day). It is possible that the extent of cross-linking within a 10BL film is less than 8 and 6 bilayers. The thicker 10BL film makes it more difficult for glutaraldehyde molecules to diffuse through the entire film thickness. In general, thicker films exhibit lower oxygen transmission rates. A thicker film has a longer diffusion pathway, which takes longer for oxygen molecules to travel through and causes them to have more interactions (e.g., H-bonding with the polymers). By increasing the number of bilayers from 6 to 8, the OTR is improved by more than 3 orders of magnitude. The significant OTR difference between 6 and 8 bilayers is largely due to the exponential growth of PEI/PAA (i.e., greater thickness). It is assumed that the films swell at 100% RH,[70,71] which enhances free volume and subsequently increases OTR. Cross-linking creates covalent bonding network, reducing the moisture sensitivity of these films, which allows better OTR under 100% RH for

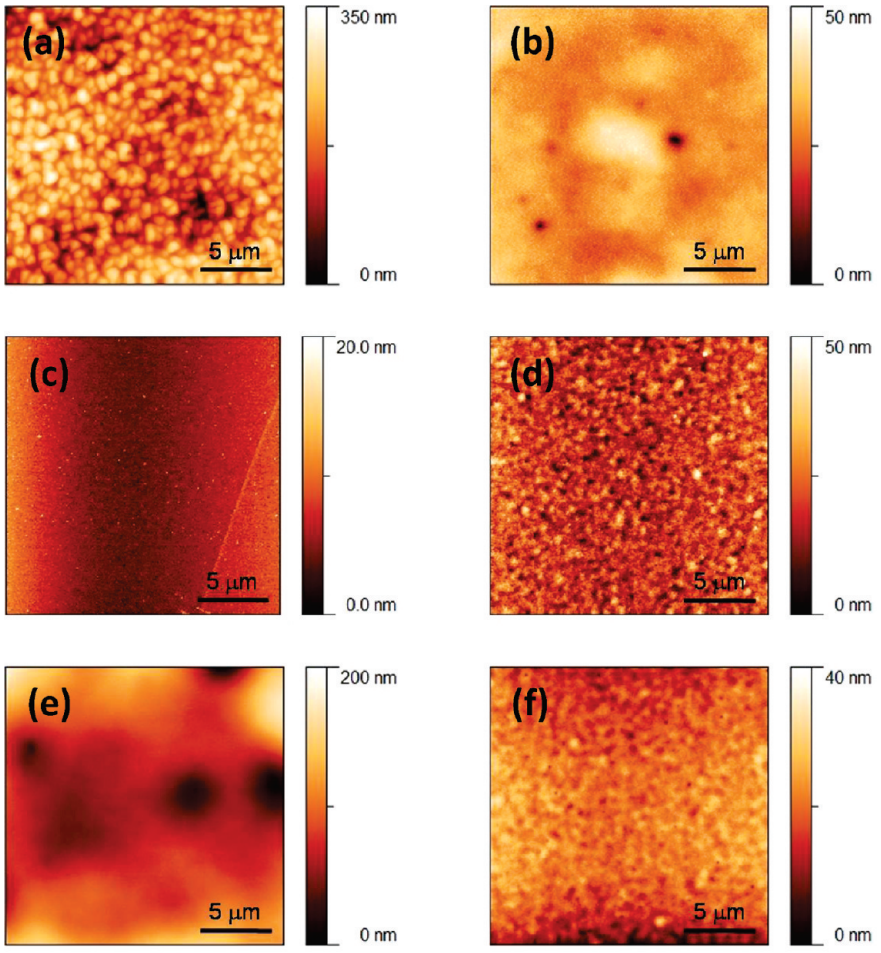

Figure 7. AFM height images of $(PEI/PAA)_{10}$ on Si wafers: PEI_{10}/PAA_4 (a), PEI_8/PAA_6 (b), PEI_7/PAA_7 (c), and PEI_4/PAA_4 (d). Two PEI-terminated surfaces, $(PEI_{10}/PAA_4)_{10.5}$ (e) and $(PEI_4/PAA_4)_{10.5}$ (f), are also shown.

Table 1. Oxygen Permeability of PEI_{10}/PAA_4 Assemblies on PET Film at 23 °C

	OTR ($cm^3/(m^2$ day atm))			permeability ($\times 10^{-16}$ cm^3 cm/(cm^2 s Pa))	
recipe	0% RH	100% RH	film thickness (nm)	film[a]	total
bare PET	8.48	8.48	N/A	N/A	17.3
$(PEI_{10}/PAA_4)_{10}$	<0.005[b]	<0.005	1080	<0.00006[b]	<0.0096
$(PEI_{10}/PAA_4)_{10}$ + CL	<0.005	0.07	680	<0.0004	<0.0096
$(PEI_{10}/PAA_4)_8$	<0.005	0.61	451	<0.000048	<0.0096
$(PEI_{10}/PAA_4)_8$ + CL	<0.005	0.09	305	<0.000032	<0.0096
$(PEI_{10}/PAA_4)_6$	3.75	3.83	369	0.057	7.70
$(PEI_{10}/PAA_4)_6$ + CL	0.56	0.17	231	0.0032	1.15

[a] Film permeability was decoupled from the total permeability using a previously described method.[81] [b] The low end detection limit for an Ox Tran 2/21 L module is 0.005 $cm^3/(m^2$ day).

both 8BL (from 0.61 to 0.09 $cm^3/(m^2$ day)) and 6BL (from 3.83 to 0.17 $cm^3/(m^2$ day)) films. Reduced thickness and incomplete cross-linking may combine to produce the increased OTR observed for the cross-linked 10 BL film.

Polyelectrolyte complexes can exhibit two extreme morphologies: a "ladderlike" structure or a "scrambled egg" structure.[72] The former is composed of two polyelectrolytes orderly packed by mutual charge compensation with cooperative effects, which is most favorable in a 1:1 stoichiometry of linear components. The scrambled egg structure is composed of randomly aggregated and oppositely charged polyions with partial charge compensation. The remaining ionic sites are charge-compensated by other counterions. On the basis of the composition, thickness, and microstructure data presented here, the PEI_{10}/PAA_4 film is believed to be closer to the scrambled egg structure, something akin to a highly interpenetrating network.[73] PEI with positively charged (or basic) amine groups always needs to stay with negatively charged (or acidic) groups from PAA for charge

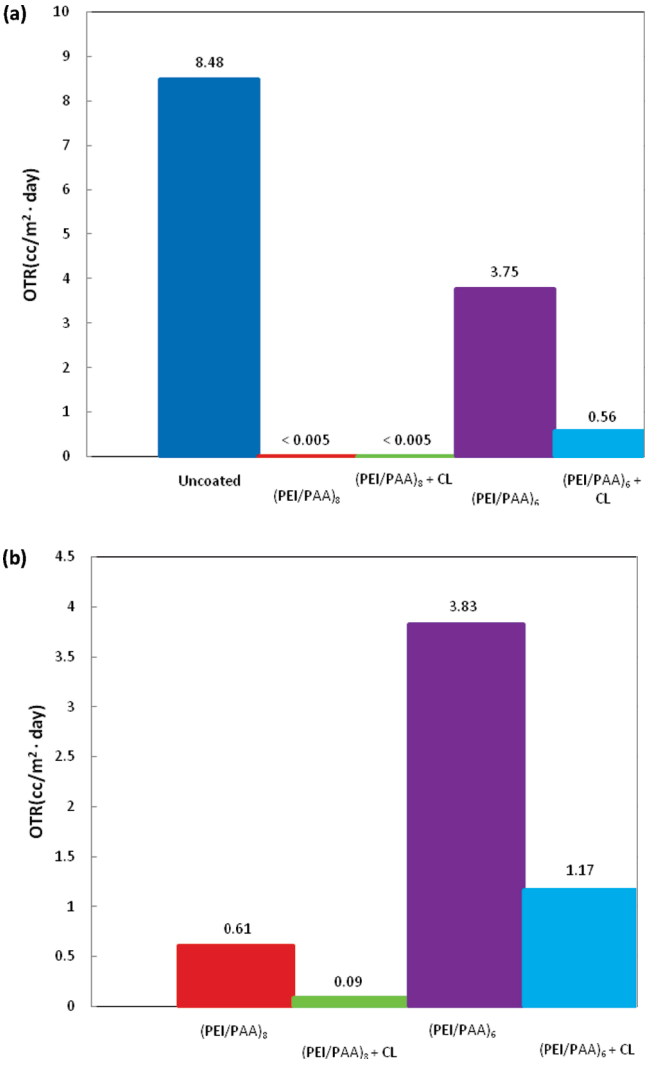

Figure 8. Oxygen transmission rate of PEI_{10}/PAA_4 films on PET at 0% (a) and 100% RH (b).

compensation. This necessary association creates numerous cation/anion (or acid/base) interfaces that contribute to a densely packed thin film.

Figure 9 shows the T_g (measured by DSC) of neat PEI, PAA, and a $(PEI_{10}/PAA_4)_{200}$ free-standing film. The weight fraction of $(PEI_{10}/PAA_4)_{200}$ was estimated from extrapolated QCM results. PEI has a T_g of −25.6 °C, and PAA has a T_g of 89.4 °C. T_g of the LbL film is higher than the linear additive combination of neat polymer T_g's, indicating that the polymer chains are more restrained inside of this network. The parallel additive model, known as the Fox equation ($1/T_{g,film} = w_{PEI}/T_{g,PEI} + w_{PAA}/T_{g,PAA}$, where w's are weight fractions of a given polymer),[74] is a reasaonable approximation for random copolymers and homogeneous polymer blends. The series model, known as the Wood equation ($T_{g,film} = w_{PEI}T_{g,PEI} + w_{PAA}T_{g,PAA}$),[75] is typically an overapproximation for copolymers and polymer blends. A positive deviation in T_g relative to these linear combination predictions can be attributed to intermolecular hydrogen bonding between these blended polymers.[76] In the case of assembled film, the dense scrambled egg structure has numerous interfaces between PEI and PAA. Moreover, hydrogen bonding between uncharged amine groups of PEI and hydroxyl groups of PAA

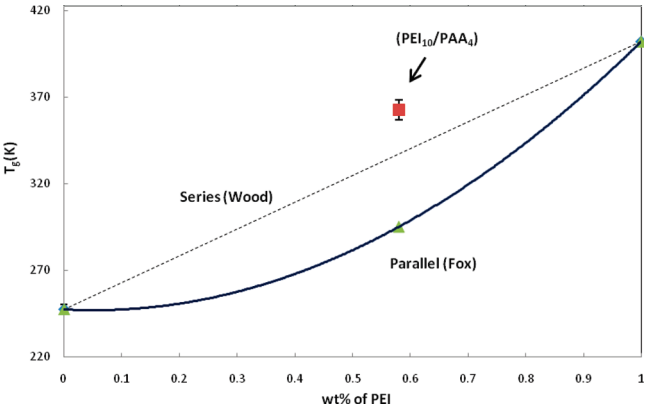

Figure 9. Glass transition temperature of PEI_{10}/PAA_4 compared to series (dotted line) and parallel (solid line) combinations of the two neat polymers. The light triangle on the parallel line is the film T_g calculated using the Fox equation.

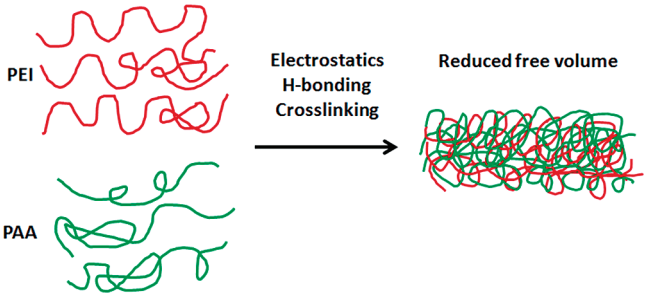

Figure 10. Schematic of reduced free volume in highly interdiffused PEI/PAA assemblies.

further decreases the mobility of each polymer, forming a more compact structure with a smaller free volume than normal polymeric membranes.[77]

A schematic illustration of the scrambled polymer blend is shown in Figure 10. In the PEI/PAA thin film, polymer chains are confined to a smaller volume than ordinary polymer blends due to the strong electrostatic attractions, intermolecular H-bonding, and/or cross-linking. The resulting densely packed structure is the believed source of low permeability in these films. Ellipsometry reveals that the highest barrier (PEI_{10}/PAA_4) films have a higher refractive index (RI = 1.65 for an 8BL assembly) than any of the other pH combinations (RI ∼ 1.45 at 8BL), which is suggestive of this more dense structure.

The relationship between permeability and free volume can be described by

$$P = A \exp\left(\frac{-B}{f}\right) \quad (1)$$

where A and B are constants that depend on the type of gas molecule. The fractional free volume, f, is defined as

$$f = \frac{V - V_0}{V} \quad (2)$$

where V is the volume of the polymer matrix and V_0 is the volume occupied by the polymer chains. Greater film density suggests the fractional free volume of this film would be relatively small, which in turn reduces permeability (density of $(PEI_{10}/PAA_4)_{20}$

$\sim$ 1.13 g/cm^3, where densities of PEI and PAA are 1.03 and 1.14 g/cm^3, respectively). The reduced thickness in cross-linked films suggests an even greater density.

Other than free volume effects, hydrogen bonding between uncharged amine groups of PEI and hydroxyl groups of PAA surely contributes some barrier to oxygen.[78,79] The permeability values in Table 1 were obtained by multiplying film thickness by OTR. The cross-linked $(PEI_{10}/PAA_4)_8$ assemblies have an unprecedented oxygen permeability ($<3.2 \times 10^{-21}$ cm^3 (STP) cm/(cm^2 s Pa) at 23 °C and 0% RH). Compared to a commercial SiO_x-coated PET, whose permeability is around 3×10^{-18} cm^3 (STP) cm/(cm^2 s Pa),[80] the permeability of the cross-linked $(PEI_{10}/PAA_4)_8$ film is 3 orders of magnitude lower. This is believed to be the lowest gas permeability ever reported for an all-polymer film of any type.

CONCLUSION

Layer-by-layer assembly of PEI and PAA was performed with various pH combinations that demonstrated the thickness and compositional tailorability of this system. Superlinear growth is observed regardless of pH. Cross-linking these films with glutaraldehyde suppresses film growth by consuming the free amine groups of PEI, which successfully inhibits polymer difussion into underlying layers. AFM images show that the surface of these films can be controlled by the outmost layer and its degree of ionization, with low pH (i.e., highly charged) PEI creating the smoothest surfaces. TEM images show homogeneous cross sections, which suggests an interpenetrating network of PEI and PAA. Oxygen permeability of cross-linked $(PEI_{10}/PAA_4)_8$ is less than 3.2×10^{-21} cm^3 (STP) cm/(cm^2 s Pa) at a thickness of just 305 nm. The superior oxygen permeability of this all-polymer assembly can be attributed to a small free volume and the numerous interfaces created by the interpenetrating network, hydrogen bonding, and cross-linking. Positive deviation of T_g (from the predictions of the Fox and Wood equations) for the LbL film confirms a strong association between PEI and PAA. This study marks the first all-polymer LbL assembly ever reported for oxygen barrier, which could be useful for food packaging, selective gas membranes, and protection of flexible electronics.

AUTHOR INFORMATION

Corresponding Author

*Tel +1 979 845 3027; fax +1 979 862 3989; e-mail jgrunlan@tamu.edu.

ACKNOWLEDGMENT

The authors thank the Texas Engineering Experiment Station (TEES) and Baker Hughes for financial support of this research. We also thank Dr. Nicole Zacharia and Dr. Sergei Nazarenko for helpful discussions.

REFERENCES

(1) Decher, G.; Hong, J. D. *Makromol. Chem., Macromol. Symp.* **1991**, *46*, 321–327.
(2) Decher, G.; Hong, J. D.; Schmitt, J. *Thin Solid Films* **1992**, *210* (1−2), 831–835.
(3) Bertrand, P.; Jonas, A.; Laschewsky, A.; Legras, R. *Macromol. Rapid Commun.* **2000**, *21* (7), 319–348.
(4) Hammond, P. T. *Adv. Mater.* **2004**, *16* (15), 1271–1293.
(5) Tang, Z. Y.; Wang, Y.; Podsiadlo, P.; Kotov, N. A. *Adv. Mater.* **2006**, *18* (24), 3203–3224.
(6) Picart, C.; Mutterer, J.; Richert, L.; Luo, Y.; Prestwich, G. D.; Schaaf, P.; Voegel, J. C.; Lavalle, P. *Proc. Natl. Acad. Sci. U.S.A.* **2002**, *99* (20), 12531–12535.
(7) Lvov, Y.; Decher, G.; Mohwald, H. *Langmuir* **1993**, *9* (2), 481–486.
(8) Yoo, D.; Shiratori, S. S.; Rubner, M. F. *Macromolecules* **1998**, *31* (13), 4309–4318.
(9) Franzl, T.; Koktysh, D. S.; Klar, T. A.; Rogach, A. L.; Feldmann, J.; Gaponik, N. *Appl. Phys. Lett.* **2004**, *84* (15), 2904–2906.
(10) Jaffar, S.; Nam, K. T.; Khademhosseini, A.; Xing, J.; Langer, R. S.; Belcher, A. M. *Nano Lett.* **2004**, *4* (8), 1421–1425.
(11) Huang, Y.; Duan, X. F.; Wei, Q. Q.; Lieber, C. M. *Science* **2001**, *291* (5504), 630–633.
(12) Kotov, N. A.; Dekany, I.; Fendler, J. H. *J. Phys. Chem.* **1995**, *99* (35), 13065–13069.
(13) Caruso, R. A.; Susha, A.; Caruso, F. *Chem. Mater.* **2001**, *13* (2), 400–409.
(14) Gole, A.; Murphy, C. J. *Chem. Mater.* **2005**, *17* (6), 1325–1330.
(15) Weintraub, B.; Chang, S.; Singamaneni, S.; Han, W. H.; Choi, Y. J.; Bae, J. H.; Kirkham, M.; Tsukruk, V. V.; Deng, Y. L. *Nanotechnology* **2008**.
(16) Aroca, R. F.; Goulet, P. J. G.; dos Santos, D. S.; Alvarez-Puebla, R. A.; Oliveira, O. N. *Anal. Chem.* **2005**, *77* (2), 378–382.
(17) Mamedov, A. A.; Kotov, N. A.; Prato, M.; Guldi, D. M.; Wicksted, J. P.; Hirsch, A. *Nature Mater.* **2002**, *1* (3), 190–194.
(18) Ma, R. Z.; Sasaki, T.; Bando, Y. *J. Am. Chem. Soc.* **2004**, *126* (33), 10382–10388.
(19) Keller, S. W.; Kim, H. N.; Mallouk, T. E. *J. Am. Chem. Soc.* **1994**, *116* (19), 8817–8818.
(20) Zhang, S. C.; Shen, J. D.; Fu, H. B.; Dong, W. Y.; Zheng, Z. J.; Shi, L. Y. *J. Solid State Chem.* **2007**, *180* (4), 1456–1463.
(21) Ariga, K.; Lvov, Y.; Kunitake, T. *J. Am. Chem. Soc.* **1997**, *119* (9), 2224–2231.
(22) Tsukruk, V. V.; Rinderspacher, F.; Bliznyuk, V. N. *Langmuir* **1997**, *13* (8), 2171–2176.
(23) Araki, K.; Wagner, M. J.; Wrighton, M. S. *Langmuir* **1996**, *12* (22), 5393–5398.
(24) Guldi, D. M.; Pellarini, F.; Prato, M.; Granito, C.; Troisi, L. *Nano Lett.* **2002**, *2* (9), 965–968.
(25) Richert, L.; Lavalle, P.; Payan, E.; Shu, X. Z.; Prestwich, G. D.; Stoltz, J. F.; Schaaf, P.; Voegel, J. C.; Picart, C. *Langmuir* **2004**, *20* (2), 448–458.
(26) Haynie, D. T.; Balkundi, S.; Palath, N.; Chakravarthula, K.; Dave, K. *Langmuir* **2004**, *20* (11), 4540–4547.
(27) Lvov, Y. M.; Lu, Z. Q.; Schenkman, J. B.; Zu, X. L.; Rusling, J. F. *J. Am. Chem. Soc.* **1998**, *120* (17), 4073–4080.
(28) Lvov, Y.; Ariga, K.; Ichinose, I.; Kunitake, T. *J. Am. Chem. Soc.* **1995**, *117* (22), 6117–6123.
(29) Toellner, L.; Fischlechner, M.; Ferko, B.; Grabherr, R. M.; Donath, E. *Clin. Chem.* **2006**, *52* (8), 1575–1583.
(30) Ladam, G.; Schaaf, P.; Decher, G.; Voegel, J. C.; Cuisinier, F. J. G. *Biomol. Eng.* **2002**, *19* (2−6), 273–280.
(31) Dimitrova, M.; Arntz, Y.; Lavalle, P.; Meyer, F.; Wolf, M.; Schuster, C.; Haikel, Y.; Voegel, J. C.; Ogier, J. *Adv. Funct. Mater.* **2007**, *17* (2), 233–245.
(32) Shimazaki, Y.; Nakamura, R.; Ito, S.; Yamamoto, M. *Langmuir* **2001**, *17* (3), 953–956.
(33) Sui, Z. J.; Salloum, D.; Schlenoff, J. B. *Langmuir* **2003**, *19* (6), 2491–2495.
(34) Ferreira, M.; Rubner, M. F. *Macromolecules* **1995**, *28* (21), 7107–7114.
(35) Mermut, O.; Barrett, C. J. *J. Phys. Chem. B* **2003**, *107* (11), 2525–2530.
(36) Shiratori, S. S.; Rubner, M. F. *Macromolecules* **2000**, *33* (11), 4213–4219.
(37) McAloney, R. A.; Sinyor, M.; Dudnik, V.; Goh, M. C. *Langmuir* **2001**, *17* (21), 6655–6663.

(38) Buscher, K.; Graf, K.; Ahrens, H.; Helm, C. A. *Langmuir* **2002**, *18* (9), 3585–3591.
(39) Tan, H. L.; McMurdo, M. J.; Pan, G. Q.; Van Patten, P. G. *Langmuir* **2003**, *19* (22), 9311–9314.
(40) Podsiadlo, P.; Michel, M.; Lee, J.; Verploegen, E.; Kam, N. W. S.; Ball, V.; Lee, J.; Qi, Y.; Hart, A. J.; Hammond, P. T.; Kotov, N. A. *Nano Lett.* **2008**, *8* (6), 1762–1770.
(41) Yang, Y. H.; Malek, F. A.; Grunlan, J. C. *Ind. Eng. Chem. Res.* **2010**, *49* (18), 8501–8509.
(42) Priolo, M. A.; Gamboa, D.; Grunlan, J. C. *ACS Appl. Mater. Interfaces* **2010**, *2* (1), 312–320.
(43) Zhai, L.; Cebeci, F. C.; Cohen, R. E.; Rubner, M. F. *Nano Lett.* **2004**, *4* (7), 1349–1353.
(44) Zhang, L.; Sun, J. Q. *Macromolecules* **2010**, *43* (5), 2413–2420.
(45) Ogawa, T.; Ding, B.; Sone, Y.; Shiratori, S. *Nanotechnology* **2007**.
(46) Podsiadlo, P.; Paternel, S.; Rouillard, J. M.; Zhang, Z. F.; Lee, J.; Lee, J. W.; Gulari, L.; Kotov, N. A. *Langmuir* **2005**, *21* (25), 11915–11921.
(47) Dvoracek, C. M.; Sukhonosova, G.; Benedik, M. J.; Grunlan, J. C. *Langmuir* **2009**, *25* (17), 10322–10328.
(48) Etienne, O.; Gasnier, C.; Taddei, C.; Voegel, J. C.; Aunis, D.; Schaaf, P.; Metz-Boutigue, M. H.; Bolcato-Bellemin, A. L.; Egles, C. *Biomaterials* **2005**, *26* (33), 6704–6712.
(49) Kim, B. S.; Park, S. W.; Hammond, P. T. *ACS Nano* **2008**, *2* (2), 386–392.
(50) Chung, A. J.; Rubner, M. F. *Langmuir* **2002**, *18* (4), 1176–1183.
(51) Quinn, J. F.; Caruso, F. *Macromolecules* **2005**, *38* (8), 3414–3419.
(52) Daiko, Y.; Katagiri, K.; Matsuda, A. *Chem. Mater.* **2008**, *20* (20), 6405–6409.
(53) Park, Y. T.; Ham, A. Y.; Grunlan, J. C. *J. Phys. Chem. C* **2010**, *114* (14), 6325–6333.
(54) Park, J.; Fouche, L. D.; Hammond, P. T. *Adv. Mater.* **2005**, *17* (21), 2575–+.
(55) Cho, C. Y.; Valverde, L.; Ozin, G. A.; Zacharia, N. S. *Langmuir* **2010**, *26* (16), 13637–13643.
(56) Tokuhisa, H.; Hammond, P. T. *Adv. Funct. Mater.* **2003**, *13* (11), 831–839.
(57) Yoo, P. J.; Nam, K. T.; Qi, J. F.; Lee, S. K.; Park, J.; Belcher, A. M.; Hammond, P. T. *Nature Mater.* **2006**, *5* (3), 234–240.
(58) Picart, C.; Lavalle, P.; Hubert, P.; Cuisinier, F. J. G.; Decher, G.; Schaaf, P.; Voegel, J. C. *Langmuir* **2001**, *17* (23), 7414–7424.
(59) Porcel, C.; Lavalle, P.; Decher, G.; Senger, B.; Voegel, J. C.; Schaaf, P. *Langmuir* **2007**, *23* (4), 1898–1904.
(60) Laugel, N.; Betscha, C.; Winterhalter, M.; Voegel, J. C.; Schaaf, P.; Ball, V. *J. Phys. Chem. B* **2006**, *110* (39), 19443–19449.
(61) Mendelsohn, J. D.; Barrett, C. J.; Chan, V. V.; Pal, A. J.; Mayes, A. M.; Rubner, M. F. *Langmuir* **2000**, *16* (11), 5017–5023.
(62) Choi, J.; Rubner, M. F. *Macromolecules* **2005**, *38* (1), 116–124.
(63) Liston, E. M.; Martinu, L.; Wertheimer, M. R. *J. Adhes. Sci. Technol.* **1993**, *7* (10), 1091–1127.
(64) Jang, W. S.; Grunlan, J. C. *Rev. Sci. Instrum.* **2005**.
(65) Gamboa, D.; Priolo, M. A.; Ham, A.; Grunlan, J. C. *Rev. Sci. Instrum.* **2010**, *81* (3), 036103.
(66) ASTM D3985-05 Standard Test Method for Oxygen Gas Transmission Rate Through Plastic Film and Sheeting Using a Coulometric Sensor. ASTM International, West Conshohocken, PA, 2005.
(67) Farris, S.; Song, J. H.; Huang, Q. R. *J. Agric. Food Chem.* **2010**, *58* (2), 998–1003.
(68) Zacharia, N. S.; DeLongchamp, D. M.; Modestino, M.; Hammond, P. T. *Macromolecules* **2007**, *40* (5), 1598–1603.
(69) Garza, J. M.; Schaaf, P.; Muller, S.; Ball, V.; Stoltz, J. F.; Voegel, J. C.; Lavalle, P. *Langmuir* **2004**, *20* (17), 7298–7302.
(70) Nolte, A. J.; Treat, N. D.; Cohen, R. E.; Rubner, M. F. *Macromolecules* **2008**, *41* (15), 5793–5798.
(71) Wong, J. E.; Rehfeldt, F.; Hanni, P.; Tanaka, M.; Klitzing, R. V. *Macromolecules* **2004**, *37* (19), 7285–7289.
(72) Philipp, B.; Dautzenberg, H.; Linow, K. J.; Kotz, J.; Dawydoff, W. *Prog. Polym. Sci.* **1989**, *14* (1), 91–172.
(73) Aoki, T.; Kawashima, M.; Katono, H.; Sanui, K.; Ogata, N.; Okano, T.; Sakurai, Y. *Macromolecules* **1994**, *27* (4), 947–952.
(74) Fox, T. G. *Bull. Am. Phys. Soc.* **1956**, *1* (2), 123.
(75) Wood, L. A. *J. Polym. Sci.* **1958**, *28* (117), 319–330.
(76) Jiang, M.; Li, M.; Xiang, M. L.; Zhou, H. *Polym. Synth.—Polym.-Polym. Complexation* **1999**, *146*, 121–196.
(77) Levasalmi, J. M.; McCarthy, T. J. *Macromolecules* **1997**, *30* (6), 1752–1757.
(78) Liou, C. C.; Wu, H. F.; Brodbelt, J. S. *J. Am. Soc. Mass Spectrom.* **1994**, *5* (4), 260–273.
(79) Lagaron, J. M.; Gimenez, E.; Catala, R.; Gavara, R. *Macromol. Chem. Phys.* **2003**, *204* (4), 704–713.
(80) Jiang, J.; Benter, M.; Taboryski, R.; Bechgaard, K. *J. Appl. Polym. Sci.* **2010**, *115* (5), 2767–2772.
(81) Roberts, A. P.; Henry, B. M.; Sutton, A. P.; Grovenor, C. R. M.; Briggs, G. A. D.; Miyamoto, T.; Kano, A.; Tsukahara, Y.; Yanaka, M. *J. Membr. Sci.* **2002**, *208* (1−2), 75–88.